3.4 Ring Impedance

Interaction of the electron beam with the surrounding vacuum chamber of the storage ring produces longitudinal and transverse wake fields. These fields are sources of extra energy spread and transverse kick for the particles in the beam. The main sources of the wake fields in storage rings are

- Finite conductivity in the material of the wall;
- Roughness of the chamber surface;
- Discontinuities in the chamber geometry due to transitions;
- Bellows and Beam Position Monitors;
- High order mode excitation in RF cavities.

The knowledge of the storage ring impedance, or the Fourier transform of the excited fields, defines the stability of the circulating electron beam. This study is the basis for the optimization of the vacuum chamber geometry, the chamber material, method of surface treatment, optimization of RF cavities design and the development of technique to suppress of the resonant terms in complete impedance.

3.4.1 Resistive Wall Impedance

It is well known [1-5], that the behavior of wake potentials induced in a round pipe of finite conductivity is determined by the characteristic distance s_0 [3] that depends on the pipe radius b and the conductivity σ. For long bunches, when the bunch length σ_z is large compare to s_0, the impedance of the chamber is dominated by the low frequency part. The longitudinal W_z and transverse W_r wake potentials of point charge are given by [2]

$$W_z(s) = \frac{1}{4\pi\varepsilon_0\sqrt{\pi Z_0\sigma}}\frac{1}{bs^{3/2}},$$

$$W_r(s) = \frac{1}{\pi^{3/2}\varepsilon_0\sqrt{\pi Z_0\sigma}}\frac{r}{b^3}\frac{1}{s^{1/2}} \qquad (3.4.1)$$

where Z_0=377 Ω is vacuum impedance, $\varepsilon_0 = 1/(36\pi 10^9) C/Vm$ is vacuum dielectric constant. Table 3.4.1 presents the characteristic distance s_0 for a round pipe of radius b=20mm of different materials. The study performed with impedance high frequency contribution into induced wake potential shows that the long wavelength approximation is valid for the bunch rms length $\sigma_z \geq 4s_0$ [4,5]. The rms bunch length for the 3 GeV electron beam is σ_z = 6.5mm, and the long-range approach for the induced fields well describe the situation. For a Gaussian bunch the potential is given by convolution of the point wake potential and the bunch longitudinal distribution [4]. The contribution of the short-range wake for CANDLE vacuum chamber is an order of 10^{-4} (Table 3.4.1). The rms

energy spread, longitudinal and transverse loss factors of the Gaussian bunch can be then presented in MKS units as

$$\sigma_\varepsilon = 0.136\left[\frac{V\cdot m}{nC\cdot\Omega^{1/2}}\right]\frac{eQ}{b\sigma_z^{3/2}\sigma^{1/2}},$$

$$k_z = 2.522\left[\frac{V\cdot m}{nC\cdot\Omega^{1/2}}\right]\frac{1}{b\sigma_z^{3/2}\sigma^{1/2}}, \qquad (3.4.2)$$

$$k_r = 0.756\left[\frac{V\cdot m}{nC\cdot\Omega^{1/2}}\right]\frac{r}{b^3\sigma_z^{3/2}\sigma^{1/2}},$$

where Q and e are the bunch and electron charges.

Table 3.4.1 Summary of the material properties

Material	**Conductivity σ ($10^7\,\Omega^{-1}m^{-1}$)**	**Characteristic distance s_0 (mm)**	**Short-range wake correction**
Stainless Steel	0.14	0.12	$2\cdot10^{-3}$
Aluminum	3.65	0.041	$4\cdot10^{-4}$
Copper	5.93	0.035	$3.2\cdot10^{-4}$

The beam energy spread and power loss in CANDLE is given in Table 3.4.2 for a bunch charge 0.7nC, which corresponding to 350 mA circulating current when all 360 RF buckets of the ring are filled.

Table 3.4.2 Energy and power loss in resistive chamber.

Material	**SS**	**Al**	**Cu**	**Units**
Power dissipation per unit length	2.05	0.41	0.32	W/m
Power loss per revolution	0.44	0.09	0.07	KW
RMS energy spread	9.59	2.49	2.08	eV/m
Energy loss	18.10	5.28	4.45	eV/m
RMS energy spread per unit charge	13.70	3.56	2.97	eV/nC/m
Energy loss Per unit charge	25.80	7.54	6.36	eV/nC/m

The maximum effect on the bunch characteristics and maximum power loss are observed for a stainless steel vacuum chamber. All cited above characteristics for stainless steel chamber are in average five times larger than for copper chamber. The longitudinal and transverse resistive wake potentials induced in CANDLE vacuum chamber are presented in Fig.3.4.1. The potentials are given for the following chamber materials: copper (Cu), aluminum (Al) and stainless steel (SS).

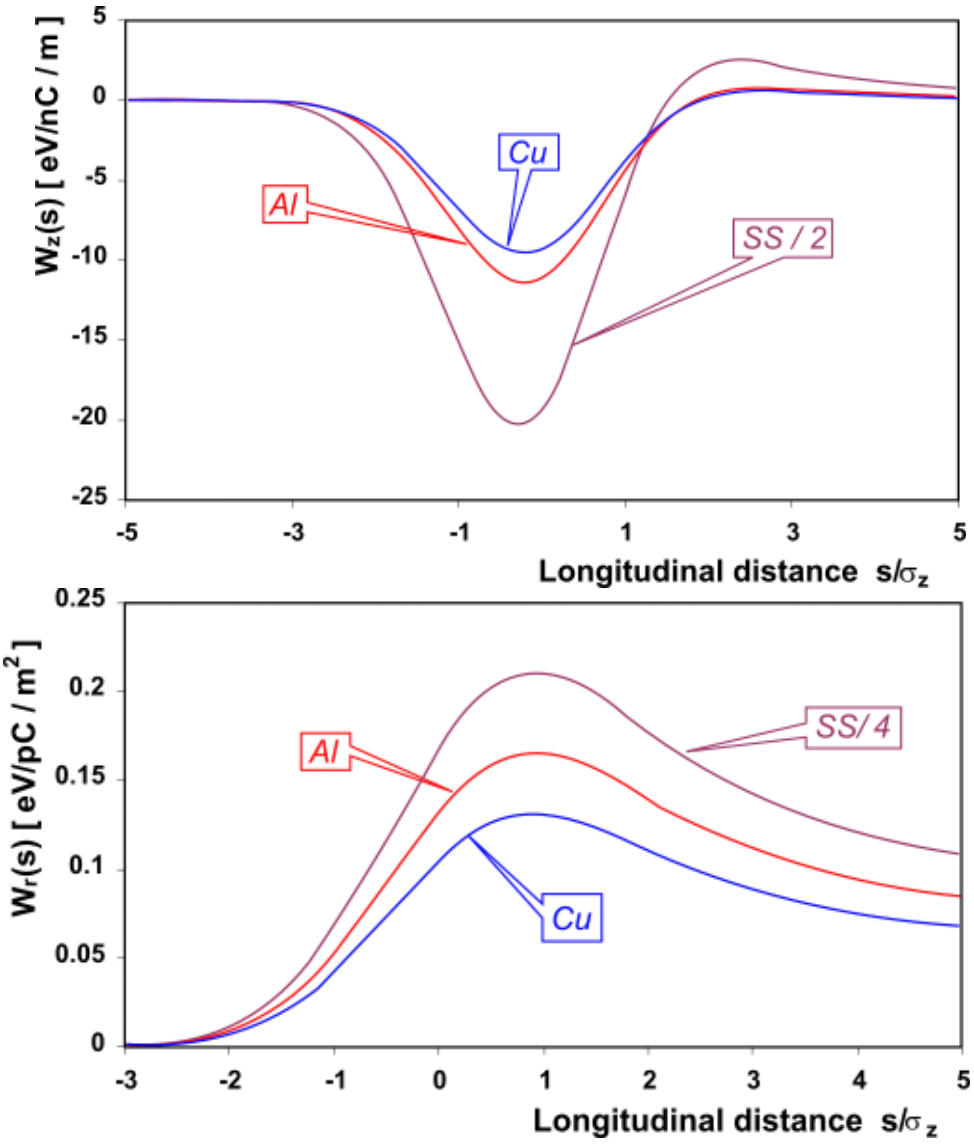

Fig.3.4.1 Longitudinal (top) and transverse (bottom) resistive wake potentials induced in CANDLE storage ring vacuum chamber .

3.4.2 Surface Roughness

The recent study performed for the TESLA-FEL beam dynamics [6-9] shows that the roughness of the vacuum chamber surface is a significant factor of the extra energy spread in the bunch that is comparable with resistive effects. The different models [6-9] for the roughness impedance have been developed to simulate this effect. An important consequence of these studies is that all the existing models predict similar results for bunch length much larger than the average size of roughness.

The most comprehensive model to simulate this effect is the Novokhatski–Timm - Weiland (NTW) model [6] when the roughness is replaced by equivalent periodic rectangular corrugations structure for the vacuum chamber walls (Fig.3.4.2).

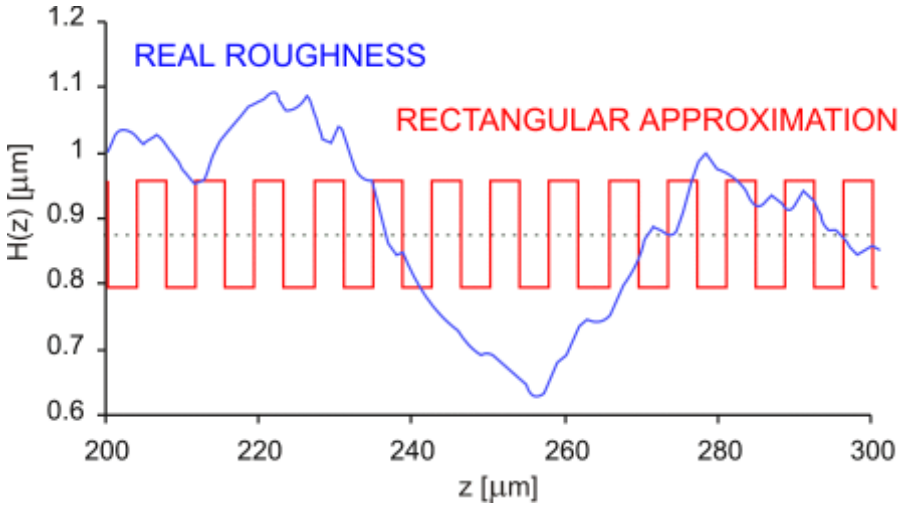

Fig. 3.4.2 The model of the periodical corrugations to describe the wall roughness.

The corresponding point charge longitudinal and transverse wake potentials are then presented as

$$w_z(s) = \frac{Z_0 c}{\pi b^2}\cos ks\,,\quad w_r(s) = \frac{2Z_0 c}{\pi b^2}\sin ks\,,\quad k = \sqrt{\frac{2p}{b\delta g}}\,, \tag{3.4.3}$$

where δ is the rms roughness size, g is the gap and p is the corrugation period, $\alpha = g/p$ is the packing factor. The analytical form of the longitudinal wake function for Gaussian bunch is then given by [9]

$$W_z(s) = -\frac{Z_0 c}{4\pi b^2} e^{-s^2/2\sigma_z^2}\left\{\xi\left(\frac{-is - k\sigma_z^2}{\sqrt{2}\sigma_z}\right) + \xi\left(\frac{-is + k\sigma_z^2}{\sqrt{2}\sigma_z}\right)\right\}, \tag{3.4.4}$$

where $\xi(x)$ is the complex error function. In the long-range approach when $\sigma_z >> \delta$ the formula (3.4.4) is converted to

$$W_z(s) = \frac{Z_0 c}{\sqrt{2\pi}k^2 b^2 \sigma_z^3} s e^{-s^2/2\sigma_z^2} \tag{3.4.5}$$

and the impedance is inductive (no power losses). However the roughness induces an energy spread within the bunch given by

$$\sigma_\varepsilon = \frac{Z_0 c}{3^{3/4}\pi^{1/2}\sigma_z^2 k^2 b^2} \tag{3.4.6}$$

A comparison of the roughness and resistive caused energy spreads is presented in Fig.3.4.3. The packing factor of the roughness is $\alpha = 0.5$. The rms energy spread for rough and resistive wakes are equal when the rms depth of roughness is equal to $\delta = 2\mu m$ for copper pipe, $\delta = 2.35\mu m$ for aluminum pipe and $\delta = 9.1\mu m$ for stainless steel vacuum chamber.

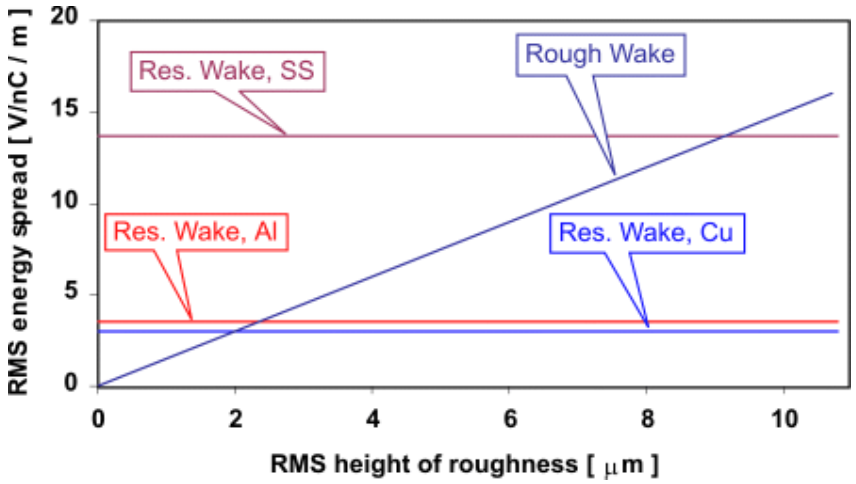

Fig. 3.4.3 RMS energy spread versus rms height of roughness. Shown the resistive energy spread for Stainless Steel, Aluminum and Copper chambers.

The corresponding longitudinal wake potentials for stainless steel vacuum chamber are shown in Fig.3.4.4.

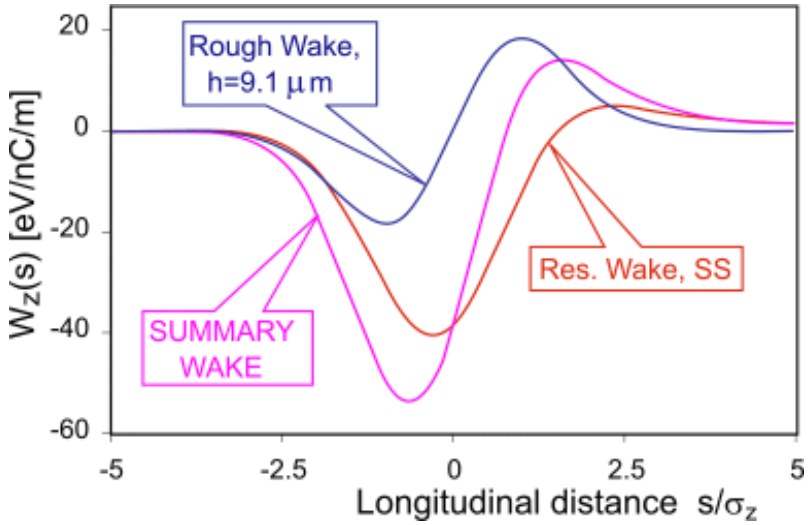

Fig. 3.4.4 The longitudinal rough, resistive and combined wake potentials for stainless steel vacuum chamber ($\delta = 9.1\mu m$).

3.4.3 Vacuum Chamber Discontinuities

The vacuum chamber discontinuities are additional sources of impedance that cause the energy spread (below cut-off frequency) and energy loss of the bunch (above cut-off frequency). The longitudinal k_z and transverse k_r loss factors for a Gaussian bunch determine the corresponding energy loss and the kick factor of the bunch. The beam power loss per turn for single element of discontinuity is given by

$$P_{lost} = k_z T_0 \frac{I_{total}^2}{N}, \qquad (3.4.7)$$

where I_{total} is the total beam current, T_0 is a revolution period and N is the number of the bunches.

Transitions. The transitions in the vacuum chamber are the transfers from the main vacuum chamber to the smaller insertion device chamber and vice versa. For the chamber transition from radius b_1 to b_2, the low frequency longitudinal and transverse components of impedance [10] and longitudinal loss factor [11] for a Gaussian bunch are given by:

$$Z_z = -\frac{i\omega Z_0}{4\pi c}\frac{d^2}{l}, \quad Z_r = -\frac{iZ_0}{2\pi}\frac{d^3}{b_1(l+d)(b_2 d + b_1 l)},$$

$$k_z = \frac{Z_0 c \ln b_2/b_1}{2\pi\sigma_z\sqrt{\pi}}\left[1 - \frac{l\sigma_z}{2d^2}\right], \tag{3.4.8}$$

where $d = b_2 - b_1$ and l is the taper length. The data given in Table 3.4.3, is calculated for $b_2 = 20mm$, $b_1 = b_2/5 = 4mm$ and $l = 7cm$.

Bellows. Bellows are sections of corrugated vacuum chamber that permit the longitudinal expansion of the rigid chambers due to temperature variations, in particular if the chambers have to be heated to high temperatures to obtain a better vacuum. The low frequency impedances and loss factor for one corrugation in bellow structure, obtained in the broadband resonance approximation, are given by [12]:

$$Z_z = i\omega\frac{gZ_0}{\pi c}\ln S, \qquad Z_r = i\frac{2gZ_0}{\pi b^2}\frac{S^2-1}{S^2+1},$$

$$k_z = \frac{gZ_0 \ln S}{4\pi^{3/2} Q\alpha^3}\frac{\omega_r^2}{c} \tag{3.4.9}$$

where δ is a corrugation depth, g is a gap width, b is a pipe radius, $S = 1 + \delta/b$, $Q \sim 3-5$ is a quality factor, $\alpha = \omega_r\sigma_z/c$ with the resonance frequency $\omega_r \sim \pi c/2\delta$. The numerical calculations performed for $\delta = 4mm$, $Q = 5$ and total gaps length $g = l/2 = 5mm$, where l is a length of bellow.

BPM's. The low frequency impedances and high frequency loss factor of the Beam Position Monitors (BPM's) of stripline split cylinder type [11,12] are given by:

$$Z_z = jZ_s\frac{\omega}{\omega_0}\frac{2l}{R}\left(\frac{\phi_0}{2\pi}\right)^2, \qquad Z_r = jZ_s\frac{c}{b^2\omega_0}\frac{2l}{R}\left(\frac{2}{\pi}\right)^2\sin^2\frac{\phi_0}{2},$$

$$k_z = \frac{Z_s c}{2\sqrt{\pi}\sigma_z}\left(\frac{\phi_0}{2\pi}\right)^2\left(1 - e^{-l^2/\sigma_z^2}\right) \tag{3.4.10}$$

Here ω_0 is the particle revolution frequency, R is the storage ring average radius, l is the stripline length, ϕ_0 is the BPM orientation angle with respect to the beam axis, Z_s is the shunt impedance at both ends of BPM. The numerical calculation (Table 3.4.3) was performed for $R = 34.4m$, $\phi_0 \sim \pi/2$, $Z_s = 5\Omega$, $l = 10cm$.

Abort Kickers. The abort kicker is a large ferrite magnet that may introduce substantial impedance at high and low frequencies. The longitudinal low frequency impedance in kickers arises due to flux leaking around edges of magnet, conductive liners etc. [12]. The longitudinal and transverse loss factors of the bunch are presented as [12]:

$$k_z = \frac{1}{2\sqrt{\pi}\sigma_z}\frac{Z_0^2}{Z_s}\frac{v^2}{c}\left(\frac{x}{a}\right)^2, \qquad k_r = \frac{Z_0 lc}{4ab\sigma_z\sqrt{\pi}} \tag{3.4.11}$$

The numerical calculation (Table 3.4.3) performed for $a = 20mm$, $b = 40mm$, $l = 6m$, $Z_s = 15\Omega$, $v = 0.04c$ and $x = 3mm$. The longitudinal and transverse loss factors, power loss per element for different type of impedance sources in CANDLE storage ring vacuum chamber are presented in Table 3.4.3.

Table 3.4.3 Loss factors for transitions

Element	**Loss factor k_z (V/pC)**	**Kick factor k_r (V/pC/m)**	**Power loss/unit (W)**
Transition	0.035	64.5	8.7
BPM	0.0036	0.95	0.9
Bellow*	0.063	20.2	15.5
Abort Kicker	0.004	16600	0.98

*without shielding

The realistic simulation of vacuum chamber impedance is possible by the using 3-dimensional code MAFIA. Nevertheless, the numerical data comparison with other light sources (SPEAR3) taking into account the difference of the bunch and vacuum chamber parameters, gives the acceptable results.

3.4.4 Impedance Summary

The equivalent presentation of different kinds of wake potentials of the bunch are characterized by frequency dependent Fourier transformations of the wake potentials, which for a Gaussian bunch may be represented as a truncated impedance:

$$\tilde{Z}(\omega) = Z(\omega)\exp\left(-\omega^2\sigma_z^2/2\right) \tag{3.4.12}$$

The main contributors to the storage ring frequency dependent total impedance, truncated by the bunch length, are given on the Figure 3.4.5 (longitudinal impedance $Z_{\|}(\omega)$) and Figure 3.4.6 (transverse impedance $Z_{\perp}(\omega)$). Shown also are the reactive Re(Z) and inductive Im(Z) parts of the total impedance.

Table 3.4.4 Impedance source parameters.

Source of wake	Quantity	Parameters
Resistive walls	-	Stainless Steel, Conductivity: 1.4 10^6 $\Omega^{-1}m^{-1}$
Roughness	-	RMS Height: 5 μ m
Transitions	6	Length: 7cm, 5:1 taper
Bellows	100	Length; 5mm; Height: 2mm
BPM	100	Length:10cm; End Impedance-5 Ω, angle $\pi/2$

The parameters used in the calculations are given in Table 3.4.4. The main influence up on the bunch parameters comes from the imaginary part of impedance and contributes the energy spread of the bunch particles. The energy losses arise from the resistive walls and transverse component of the roughness impedance. The bellows, BPM's and transition sections contributions to the total energy losses are comparatively small.

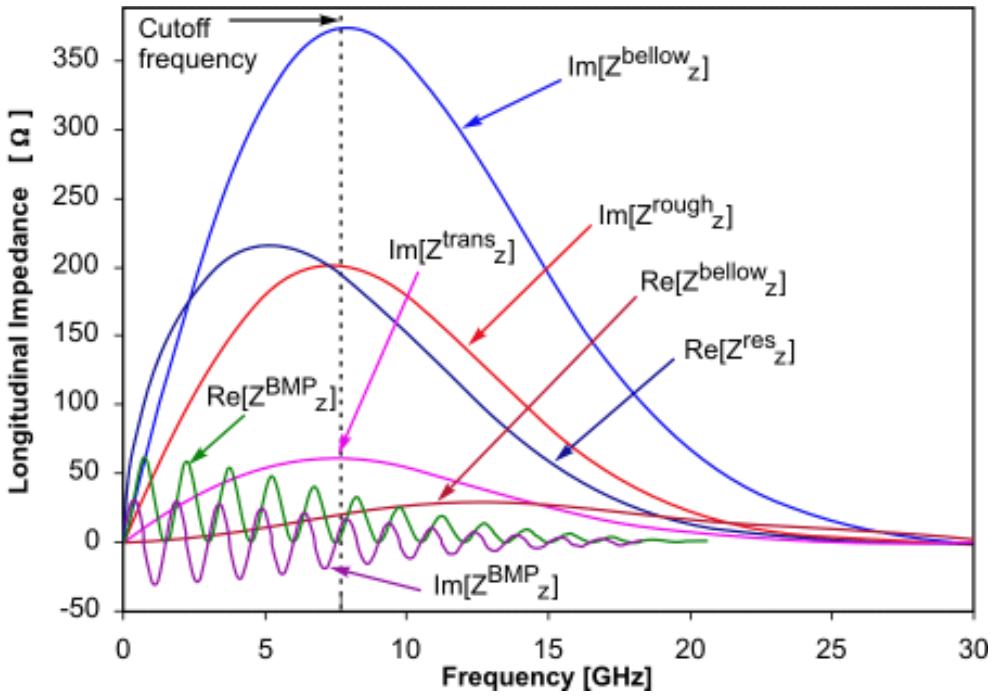

Fig.3.4.5 Longitudinal impedances of the ring caused by walls resistivity, surface roughness, BPM's, transitions and bellows.

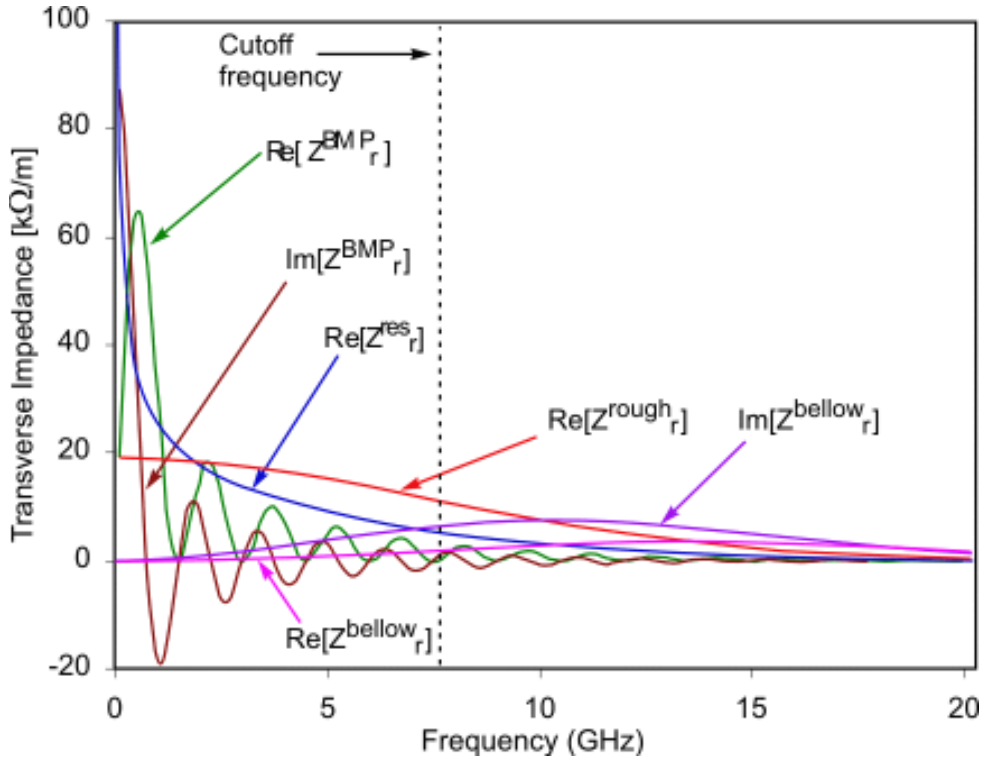

Fig.3.4.6 Transverse impedances of the ring caused by walls resistivity, surface roughness, BPM's, transitions and bellows.

Reference

1. A.W. Chao, “Physics of Collective Beam Instabilities in High Energy Accelerators”, New York, John Willey & Sons, Inc., 1993.
2. K.L.F. Bane and M Sands, “The Short-Range Resistive Wall Wakefield”, SLAC-PUB-95-7074, Dec. 1995.
3. A.Piwinski, “Wake Fields and Ohmic Losses in Round Vacuum Chambers,” DESY HERA 92-11, May 1992.
4. M.I. Ivanian, V.M.Tsakanov, “Summary of the Resistive Wake-Field Effects in TESLA-FEL Transfer Line”, TESLA-FEL 2000-25, Dec. 2000.
5. M.I. Ivanyan, V.M.Tsakanov, “The Analytical Treatment of Resistive Wake in Round Pipe”, PAC-2001, Chicago, Jun. 2001.
6. A. Novokhatsky, M. Timm, and T. Weiland, DESY-TESLA-99-17, Sep 1999. 5pp
7. K.L.F. Bane and G.V. Stupakov, “Wake of a Rough Beam Wall Surface”, SLAC-PUB-8023, Dec. 1998, 6p.
8. K.L.F. Bane, C.K. Nb and A.W. Chao, “Estimate of the Impedance Due to Wall Surface Roughness”, SLAC-PUB-7514, May 1997.
9. M. Dohlus, M.I. Ivanian, and V.M. Tsakanov, “Surface Roughness Study For The Tesla-Fel”, DESY-TESLA-FEL-00-26, Feb 2001, 11pp.
10. K.Yokoya, “Impedance of Slowly Tapered Structures”, CERN SL/90-88 (AP), 1990.
11. B. W. Zotter and S.A. Kheifets, “Impedances and Wakes in High-Energy Particle Accelerators”, Word Scientific, 1997, 406p.
12. G.R.Lambertson and K.-Y. Ng, “Beam Impedances of Position Monitors, Bellows and Abort Kickers”,. LBL-25385, SSC-N-517, FN-487, May 1988.